Proceedings of the ASME 2025 International Technical Conference and Exhibition on Packaging and Integration of Electronic and Photonic Microsystems InterPACK2025

October 28-30, 2025, Anaheim, California

IPACK2025-164089

SYSTEMATIC ANALYSIS OF THERMAL RESISTANCES IN DATA CENTERTWO-PHASE DIRECT-TO-CHIP COOLING

Qingyang Wang	Serdar Ozguc	Richard W. Bonner
Accelsius	Accelsius	Accelsius
Austin, TX	Austin, TX	Austin, TX

ABSTRACT

The surging power densities of processors and server racks in data centers have posed significant challenges to data center thermal management. Pumped two-phase (2P) direct-to-chip (DTC) cooling uses boiling of a dielectric refrigerant and is efficient, reliable, and future-proof for data center cooling. However, a comprehensive understanding and evaluation of 2P DTC within the data center community is still missing. In this work, we performed a systematic analysis of 2P DTC cooling, breaking up the end-to-end temperature difference into three thermal resistances: cold plate thermal resistance, vapor line pressure drop-induced thermal resistance, and condenser thermal resistance. We proposed to use the refrigerant temperatures at cold plate outlet and at condenser inlet as two temperature nodes to divide the end-to-end temperature difference. Notably, the condenser temperature rise is represented by a maximum temperature difference, which incorporates the effect of saturation temperature drop due to pressure drop of 2P flow across the condenser. We developed models and analysis for two 2P refrigerants (R1233zd(E) and R515B) and discussed the variations of cold plate and condenser thermal resistances with different parameters. The thermal stack-up bars for 2P DTC cooling with the two refrigerants are compared with single-phase (1P) DTC cooling, showing comparable performance between 1P and 2P with 1000 W processors and advantageous performance of 2P DTC with 2000 W processors. This work establishes a framework to break down 2PDTC thermal contributions and analyze 2PDTC components, providing theoretical support to the at-scale adoption of 2P DTC cooling in data centers.

Keywords: data center, liquid cooling, two-phase cooling, direct-to-chip, thermal resistance

NOMENCLATURE

Α	total heat transfer area, [m ²]
Во	boiling number
F_K	a fluid-dependent constant in the Kandlikar
	correlation
G_{ch}	channel mass flux, [kg/m² s]
h	heat transfer coefficient, [W/m ² K]
h_{fg}	latent heat of vaporization, [J/kg]
Nu	Nusselt number
Q	heat/power, [W]
$q_w^{\prime\prime}$	wall heat flux, [W/m ²]
R_{co}	case-to-outlet thermal resistance, [K/W]
R_{dp}	vapor line pressure-drop-induced thermal
	resistance
T	temperature, [°C]
T_{case}	case temperature, [°C]
T_{out}	refrigerant temperature at cold plate outlet,
	[°C]
U	overall heat transfer coefficient, [W/m ² K]
x	vapor quality

Greek symbols

A 7T	1 4 1	4 4 1	. cc	C	T
ΔT_{e2e}	ena-to-ena	temperature d	itterence	trom	1
	ond to ond	terriperature a	1110101100	11 0111	* Case

to $T_{FW.in}$, [°C]

 ΔT_{rise} facility water temperature rise, [°C]

 ΔT_{sat} refrigerant saturation temperature drop in the

condenser, [°C]

 ρ density, [kg/m³]

Subscripts

ave average

boil the point when refrigerant starts boiling in the

cold plate

CBD convective boiling dominant

ci the point at condenser inlet

cl the point when the refrigerant becomes

saturated liquid in the condenser

FW,in facility water inlet (supply) FW,out facility water outlet (return)

l liquid phase le liquid only

NBD nucleate boiling dominant

res reservoir sat saturation tot total heat v vapor phase

Acronyms

1P single-phase 2P two-phase

ATD approach temperature difference

CDU coolant distribution unit

DTC direct-to-chip FW facility water

HTC heat transfer coefficient

HX heat exchanger

LMTD logarithmic mean temperature difference MTD maximum temperature difference (in the 2P

condenser)
PG propylene glycol

PG25 a coolant mixture of 25% PG and 75% water

QD quick-disconnect coupling TDP thermal design power TIM thermal interface material

1. INTRODUCTION

Data centers consume over 4% of the total electricity production in the US [1], and 33~40% of that is used for cooling [2]. The power densities of server racks in data centers are increasing rapidly due to the surging demand for high-performance computing, accelerated by the development of artificial intelligence. The thermal design power (TDP) of advanced processors is also increasing across generations, with the current released high-power processors approaching or exceeding 1000 W TDP [3-5] and future processors possibly reaching 2000 W if the trend continues [6]. Efficient and reliable thermal management of data centers is of urgent need to reduce energy consumption used for cooling, and to enable advanced computing with high chip-level and rack-level power densities.

As the cooling demand pushes beyond the capabilities of traditional air convection, liquid cooling is becoming a necessity. Compared with immersion cooling, cold plate based direct-to-chip (DTC) cooling offers high performance at lower cost, and allows easier retrofit of existing air-cooled data centers. Single-phase (1P) DTC cooling using water/propylene glycol (PG) mixtures was developed and deployed for data center liquid cooling. A gradually maturing ecosystem for 1P DTC is building up from the collective efforts in the industry [7]. However, although 1P DTC provides sufficient cooling performance for the recent generations of processors, using water-based coolant

brings risks of leakage, corrosion, bio-growth, etc. Moreover, as the processor TDP and heat flux keep increasing in the future, 1P convection might require an infeasible flow rate/velocity to dissipate ultrahigh TDP/heat flux and reach its cooling capacity limit.

Two-phase (2P) boiling heat transfer offers high heat transfer coefficient (HTC), and has been extensively studied for cooling electronics. Lab-scale experiments demonstrated heat flux dissipation over 1000 W/cm² with refrigerant boiling heat transfer [8, 9]. 2P DTC cooling using dielectric refrigerant is thus a promising technology to enable cooling of high power and high heat flux processors packed in high density [10]. Different refrigerants were introduced and compared for 2P cooling [11-131. Experimental tests demonstrated dissipation of high power (>1000 W) and high heat flux (up to 300 W/cm²) at the cold plate level [6, 14-16], including under different server or cold plate orientations [17]. System-level analysis and testing have also been conducted to understand and regulate flow distribution in the highly parallel 2P flow paths [18-21]. However, 2P DTC for data center cooling is still in early development stage and has not been deployed at scale.

Compared with 1P DTC systems, 2P DTC systems are more complex due to the interdependence between temperature and pressure in a 2P loop. Currently, 2P DTC cooling for data centers is not yet understood comprehensively by the data center community. Although it has been demonstrated that a universal cold plate could be used for DTC cooling working under both 1P and 2P mode [6, 22], there is still confusion on the system-level performance of 2P DTC. There have been misunderstandings and misleading conclusions when 2P DTC cooling is compared to other liquid cooling solutions, leading to overestimation or underestimation of its performance. As 2P DTC gradually makes its way into the data center industry, there is a pressing need to establish a systematic thermal analysis for 2P DTC cooling, and offer data center engineers quick and easy methods to evaluate and compare the performance of 2P components and systems.

For data centers with a chilled facility water (FW) loop, the end-to-end temperature difference between processor case temperature T_{case} and FW inlet temperature $T_{FW,in}$ is of the most concern. In this work, we provide a comprehensive analysis of the thermal resistances existing in 2P DTC systems, identifying three thermal resistances contributing to the end-toend temperature difference. The condenser thermal resistance causes the temperature rise from $T_{FW,in}$ to refrigerant temperature entering the condenser T_{ci} , the vapor line pressure drop induced thermal resistance causes the temperature rise from T_{ci} to the cold plate outlet temperature T_{out} , and the cold plate thermal resistance causes the temperature rise from T_{out} to T_{case} . Notably, here we propose that the condenser thermal resistance should be characterized by the maximum temperature difference ($MTD = T_{ci} - T_{FW.in}$) instead of the approach temperature difference (ATD) used for 1P DTC cooling, in order to include condenser pressure drop contribution and account for the temperature mismatch in the condenser. Models are developed to estimate the temperature rise from the cold plate and the condenser, and the comparisons between two 2P refrigerants R1233zd(E) and R515B and between 1P and 2P DTC cooling are discussed. The thermal stack-up plots show that 2P cooling offers smaller end-to-end temperature difference and allows higher FW temperature when the processor power approaches 2000 W. This work establishes the metrics for performance characterization of 2P DTC cold plates and condensers, allows data center engineers to easily and fairly compare 2P DTC with other cooling technologies, and paves the way for at-scale adoption of 2P DTC cooling for data centers.

2. 2P DTC SYSTEM OVERVIEW

Although pumped 2P cooling has been widely studied and used in thermal management applications, its use in data centers is still in early development. Kulkarni et al. [23] presented an overview of pumped 2P DTC cooling for data centers. The main components of a 2P DTC system include a coolant distribution unit (CDU) (which contains the pumps and the condenser), liquid and vapor manifolds, a fluid reservoir, cold plates, and tubings/hoses/fittings/connectors. Figure 1 shows an exemplary in-rack 2P DTC system [24]. The operation of pumped 2P DTC cooling is driven by the pumps in the system, which generate pressure head and push the refrigerant to flow in a loop.

Figure 2 shows a simplified schematic of the 2P DTC system, with letters A-H marking eight characteristic status points in the operation cycle. Figure 3 is the pressure-enthalpy (p-h) diagram of the loop, showing the thermodynamic states of the refrigerant at different status points shown in Figure 2. The cycle in Figure 3 assumes adiabatic boundary conditions for the flow loop components because the heat loss is negligible compared to the system heat load. Since any flow would result in a pressure drop, Figure 3 displays the exaggerated pressure drop magnitude to include all pressure drop contributions, and the figure is not to-scale.



Figure 1: 3D Drawing of an in-rack 2P DTC cooling system [24].

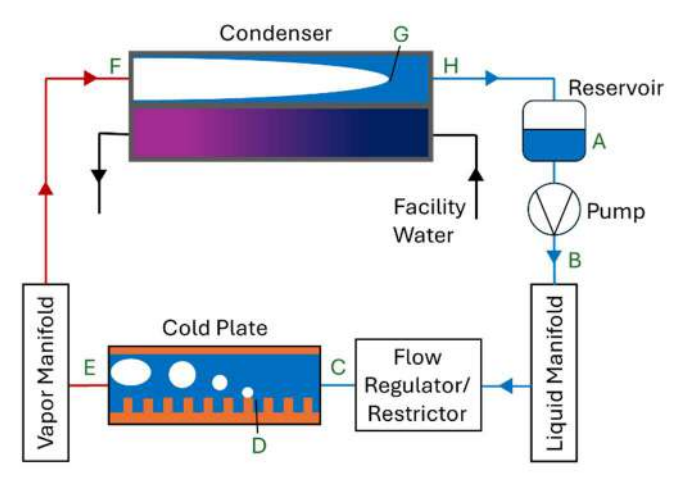


Figure 2: Schematic of a 2P DTC loop showing the close-loop refrigerant circulation.

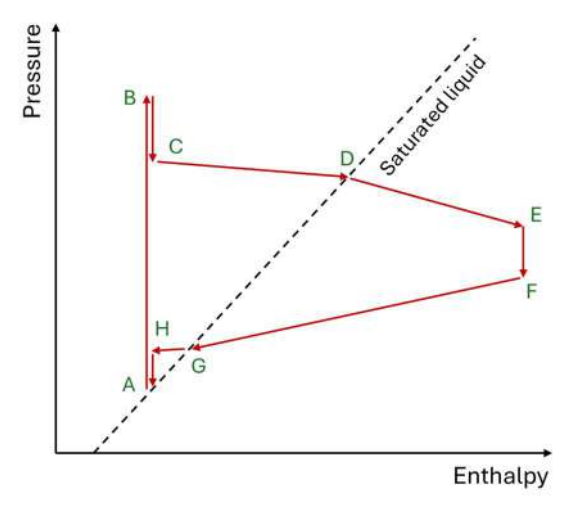


Figure 3: *p-h* diagram showing the thermodynamic states of the refrigerant in a 2P DTC loop at different status points.

The cooling cycle contains the following steps. The refrigerant is initially saturated inside the reservoir with liquidvapor coexistence. The pump pulls the saturated liquid (point A) and pressurizes it after the pump (point B). The pressurized liquid flows along the liquid line (including the particle filter, the liquid manifolds, the liquid quick-disconnect (QD), and the pressure regulator/restrictor) towards the inlet of the cold plate (point C). There is a pressure drop from B to C due to frictional or momentum pressure drop induced by the liquid line and associated components. Point C is on the left side of the saturated liquid line in Figure 3, indicating that the refrigerant is now subcooled. The subcooled liquid enters the cold plate and absorbs heat, and the thermodynamic state changes from the cold plate inlet C to the cold plate outlet E, passing the saturated liquid line at the boiling incipience point D. The saturated two-phase mixture at the cold plate outlet flows along the vapor line (including the vapor hoses/tubings, vapor QD, vapor manifolds, etc.) to the inlet of the condenser F, and its thermodynamic state

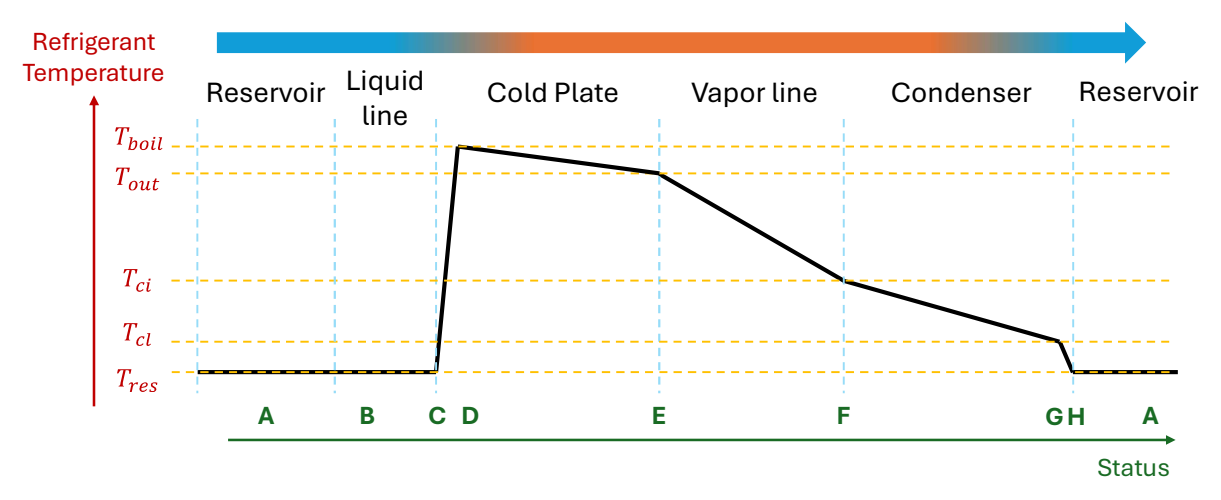


Figure 4: Refrigerant temperature variation along the loop at different status points.

changes from E to F due to vapor line pressure drop. In the condenser, the saturated two-phase mixture at condenser inlet F dumps heat to FW and becomes subcooled liquid at the condenser outlet H, passing the saturated liquid line again at point G inside the condenser. The subcooled liquid flows back to the reservoir, along which the pressure drop brings its thermodynamic state from point H back to saturated liquid at point A.

Figure 4 shows the refrigerant temperature variation along the loop. The refrigerant temperature remains T_{res} from the reservoir (point A) to the inlet of the cold plate (point C). The fluid absorbs heat inside the cold plate, first as single-phase liquid until reaching T_{boil} at point D, and then as two-phase mixture with increasing thermodynamic quality from D to cold plate outlet E. The temperature of the two-phase mixture drops from T_{boil} when boiling starts to T_{out} at the outlet, due to the two-phase pressure drop inside the cold plate. The mixture temperature drops from T_{out} at cold plate outlet E to T_{ci} at the condenser inlet F, due to pressure drop along the vapor line. As the mixture is condensed inside the condenser, it drops temperature due to two-phase pressure drop from T_{ci} to T_{cl} at point G, at which point all the vapor is condensed and the fluid becomes saturated liquid. The saturated liquid is further subcooled and reaches T_{res} at condenser outlet H, and then flows back to the reservoir without any temperature change. In Section 3.3, it will be shown that for a common 2P DTC system with reasonable assumptions, point G converges into H, and T_{cl} approaches T_{res} .

3. 2P DTC THERMAL RESISTANCES

For data center thermal management with chilled FW loop as the primary cooling loop, the end-to-end temperature difference (ΔT_{e2e}) is of the most interest, which is the difference between the chip case temperature T_{case} and the FW inlet temperature $T_{FW,in}$ [25]. The temperature rise ΔT_{e2e} represents the total thermal resistance of a cooling solution and dictates the energy consumption for cooling, and other

temperature nodes in between are of less interest to data center operators. For 2P DTC cooling, this ΔT_{e2e} is comprised of three temperature differences, corresponding to three thermal resistances resulted from different components of the system, separated by two temperature nodes T_{out} and T_{ci} between the two ends as discussed below.

3.1 Cold Plate Thermal Resistance

The case-to-fluid thermal resistance is usually used in data center cooling applications, incorporating the thermal interface material (TIM), base plate conduction, and convection/boiling. For 2P DTC cooling, Figure 4 shows that the refrigerant temperature inside the cold plate first increases from T_{res} to T_{boil} and then drops to T_{out} . In most practical conditions, the saturation temperature drop from T_{boil} to T_{out} is very small, and a constant T_{sat} is used to obtain the thermal resistance [6, 14]. On top of the constant saturation temperature assumption, some works [13] used a weighted average fluid temperature to account for the 1P fraction of heat transfer from point C to D, although the 1P contribution is mostly small and the calculated weighted average is very close to the 2P saturation temperature itself. More complex temperature profiles could exist if the cold plate has internal manifolds to distribute the flow [15]. Moreover, if the cold plate exit has certain narrow passages or sharp turns, it could also create a pressure drop and consequently a temperature drop. It is thus difficult to either model the fluid temperature distribution or experimentally measure the saturation temperature distribution within the cold plate, especially when the temperature drop inside the cold plate (including when exiting the cold plate) is not negligible.

Using temperature inside the cold plate to obtain thermal resistance would relate the thermal resistance very well with the convective/boiling HTC. Nonetheless, due to the difficulties in obtaining the actual fluid temperature (distribution) inside the cold plate, Ref. [26] proposed to use the cold plate outlet temperature to obtain 2P cold plate thermal resistance as the case-to-outlet resistance,

$$R_{co} = \frac{T_{case} - T_{out}}{Q} \tag{1}$$

which includes the pressure drop contribution into the thermal resistance value and eliminates the need to obtain an accurate fluid temperature distribution within the cold plate. In a lot of practical cases when cold plate 2P pressure drop is small and T_{out} is close to the internal saturation temperature, using T_{out} results in negligible difference from using T_{sat} ; in certain conditions when the temperature drop within the cold plate is significant, the thermal resistance can account for the temperature rise of T_{case} resulted from 2P pressure drop, by incorporating the pressure drop-induced thermal resistance. Moreover, T_{out} can be easily measured outside of the cold plate in experimental testing, thus helping facilitate R&D and quality validation of 2P cold plate products.

Therefore, following Ref. [26], in this work, the cold plate thermal resistance is represented by the temperature differential from T_{case} to T_{out} , and the cold plate outlet T_{out} at point E is taken as the first temperature node to break down the ΔT_{e2e} .

3.2 Condenser Thermal Resistance

The heat exchangers (HXs) used in DTC cooling CDUs are usually arranged in a cross-flow configuration. For 1P DTC cooling, the CDU (or HX) thermal resistance is commonly characterized by the approach temperature difference (ATD), which is the difference between the secondary coolant temperature at HX outlet and the primary coolant temperature at HX inlet. For 2P DTC cooling, the same definition can be used, representing the temperature difference between refrigerant exiting the condenser and the FW entering the condenser. Detailed modeling and quantitative analysis of the ATD variation with different working conditions will be given in Section 4.

Similar to the cold plate thermal resistance where using the saturation temperature represents the boiling HTC, from a heat transfer point of view, the condenser thermal resistance can represent the heat transfer performance better by using the logarithmic mean temperature difference (LMTD) as the characteristic temperature difference. From a data center operation point of view, ATD is of more practical interest as it relates directly to the FW inlet temperature. For 1P HXs, ATD equals LMTD when the hot fluid and cold fluid are of the same composition and flow rate. However, in a 2P condenser, the secondary coolant (refrigerant) temperature does not drop due to cooling by the primary coolant (FW). The temperature drop of refrigerant purely results from pressure drop. Consequently, the ATD value of a condenser at the approach side is usually much larger than LMTD. Meanwhile, the refrigerant temperature drop due to pressure drop is not captured by the ATD value, and a lower ATD does not always mean better condenser performance, as will be discussed in Section 4.

To incorporate the pressure drop effect into the condenser temperature rise, we suggest to use the refrigerant temperature at the condenser inlet T_{ci} (as shown in Figure 4) as the other temperature node. Hence, the difference between refrigerant inlet T_{ci} and FW inlet $T_{FW,in}$ can be used to represent condenser thermal resistance. Since the refrigerant inlet and FW

inlet represent the highest and the lowest temperatures of the hot and cold fluids, respectively, the temperature difference ($T_{ci} - T_{FW,in}$) is termed maximum temperature difference (MTD) in this work. Section 4 provides a more detailed analysis of MTD variation with different working conditions.

3.3 Pressure Drop-Induced Thermal Resistance

In 2P systems, pressure and temperature are directly correlated under saturated conditions. Thus, as the two-phase mixture exits the cold plate and flows along the vapor line and the condenser, the temperature drops along the flow due to pressure drop. This refrigerant temperature drop is manifested as an effective thermal resistance of the system.

According to Figure 4, the temperature drop associated with pressure drop is comprised of three components: T_{out} to T_{ci} in the vapor line, T_{ci} to T_{cl} (point G) inside the condenser, and T_{cl} to T_{res} . T_{cl} corresponds to point G inside the condenser when the fluid is fully condensed into saturated liquid and the thermodynamic quality reaches 1. The reason for the pressure drop from H to A in the p-h diagram (Figure 3) is purely due to the fully condensed liquid flow from condenser outlet to reservoir. In practical cases, this pressure drop is usually negligible since the fluid is purely in liquid phase and there are no flow restrictions (such as filters, QDs or sharp turns). When the pressure drop from H to A is neglected, H and A would have the same thermodynamic states, and hence point G on the saturated liquid line in the p-h diagram must coincide with point A, so that points G, H, and A converge. In other words, T_{cl} converges to T_{res} , and the condenser outlet G/H will have saturated liquid at temperature T_{res} .

The condenser pressure drop induced temperature drop can be incorporated into the MTD value as discussed above. Therefore, as the third thermal resistance, the pressure drop induced thermal resistance (R_{dP}) should only represent the temperature rise not included by the cold plate and the condenser thermal resistances, i.e., between the two temperature nodes of cold plate outlet T_{out} and condenser inlet T_{ci} , based on the discussion in Sections 3.1 and 3.2. In other words, given the thermal resistance definitions for cold plate and condenser, only the vapor line pressure drop should be considered for R_{dp} .

The vapor line pressure drop includes contributions from the tubings/hoses of in-server plumbing, QD couplings, rack- and row-level return manifolds, and hoses from return manifolds to the condenser inlet. The pressure drops from vapor line can be minimized as much as possible during server-level and system-level designs, by implementing larger flow cross-section area and removing sharp turns/bends. The design should holistically take into consideration the rated cooling power, the available physical space for the components, and the acceptable saturation temperature drop.

4. MODELING AND DISCUSSION

4.1 Cold Plate Temperature Rise

A simplified model is established to estimate cold plate temperature rise in 2P DTC systems. The model is formulated

similar to the one in Ref. [26]. A heated rectangle is considered as the case surface of a chip package with a size of 25×33 mm². Uniform heat flux conditions are assumed for a given heat load. A cold plate is attached to the heated surface, with microchannel structures on top of a base plate. The microchannels are formed by straight upright fins with 0.2 mm width, 0.2 mm spacing, and 3 mm height, consistent with typical skived-fin cold plate parameters. The footprint of the finned area matches the heated surface, with the fin length (channel length) equal to the length of the heated surface (33 mm). The cold plate has a base plate thickness of 2 mm and is made of copper with a thermal conductivity of 390 W/(m·K). A TIM with a thermal resistance of 10 mm²K/W is applied between the cold plate and the heated surface.

For 2P cold plate calculations, inlet subcooling is considered to be zero, since sensible heat contribution is usually small. A vapor exit quality of 0.7 is used to adjust the inlet flow rate according to different given TDPs. The channels are meshed into segments. Within each segment, Kandlikar correlation [27] is used to calculate the boiling HTC:

$$h = \max(h_{NBD}, h_{CBD}) \tag{2}$$

where the nucleate boiling dominant and convective boiling dominant HTCs are calculated by

inant HTCs are calculated by
$$h_{NBD} = 0.6683 \left(\frac{\rho_l}{\rho_v}\right)^{0.1} x_{ave}^{0.16} (1 - x_{ave})^{0.64} h_{le} \\ + 1058.0 Bo^{0.7} F_K (1 - x_{ave})^{0.8} h_{le} \\ h_{CBD} = 1.1360 \left(\frac{\rho_l}{\rho_v}\right)^{0.45} x_{ave}^{0.72} (1 - x_{ave})^{0.08} h_{le} \\ + 667.2 Bo^{0.7} F_K (1 - x_{ave})^{0.8} h_{le}$$

$$(3b)$$

In Eq. (3), x_{ave} is the average vapor quality along each segment. h_{le} is the liquid-only convective HTC, calculated from the Nusselt number for liquid-only channel flow. The Nu is taken as 7.25, which is the fully-developed laminar Nu given the rectangular channel cross-sectional with an aspect ratio of 15 under constant wall heat flux conditions [28]. The value of fluid-dependent parameter F_K is not available for the refrigerants being calculated, and is taken as 1 in this work [29]. The boiling number Bo is defined by

$$Bo = \frac{q_w^{"}}{G_{ch}h_{fg}} \tag{4}$$

where G_{ch} is the channel mass flux and h_{fg} is the latent heat. The wall heat flux q_w'' is calculated from the footprint heat flux and the surface area enhancement, taking into consideration the fin efficiency. The calculation is iterated until the channel HTC and fin efficiency are both converged. The 2P pressure drop along the channel includes both frictional and accelerational components. The friction pressure drop is obtained from Darcy-Weisbach equation with homogeneous flow assumption. Other details about the model can be found in Ref. [26]. In this work, a T_{out} of 40 °C is given. The case temperature T_{case} is then obtained by summing up the temperature rises of TIM, base plate conduction, boiling heat transfer, and pressure drop and adding the sum onto T_{out} . Two different dielectric fluids are modeled,

including a low-pressure refrigerant R1233zd(E) and a medium-pressure refrigerant R515B.

For comparison, the same cold plate configuration mentioned above is also modeled for 1P cooling using PG25 as the working fluid. A temperature rise of 10 °C is assumed for 1P sensible cooling, corresponding to ~1.5 L/min per kW of heat load and consistent with practical applications. The same microchannel laminar convection Nu and fin-efficiency iteration are implemented. The fluid inlet temperature is fixed at 40 °C. The wall temperature is obtained using the calculated convective HTC and the average fluid temperature between inlet and outlet temperatures. The case temperature is obtained by further adding the temperature rises from TIM and base plate conduction. It is noted that by using the average fluid temperature, the obtained case temperature is an average over the heated surface instead of the maximum.

Figure 5 shows the calculated results for the same cold plate configuration operating at both 1P and 2P modes. The case temperature is plotted as a function of the TDP given the same heated area. For both 2P refrigerants, the resulted case temperature is lower than that of the 1P case for a given TDP with the same characteristic fluid temperature of 40 °C. The temperature difference increases with TDP: for a 500 W chip, 2P yields a ~8 °C lower case temperature; for a 2000 W chip, 2P yields a ~17 °C lower case temperature. The reason is primarily due to the enhanced heat transfer performance offered by boiling with a higher HTC, and the temperature rise increases more-orless linearly with TDP, due to the almost flow rate-independent HTCs for both 1P laminar convection and 2P nucleate boiling. Moreover, 2P cooling tends to yield a uniform case surface temperature, whereas 1P cooling could have significant temperature gradient along the flow path, further expanding the temperature difference between 1P and 2P shown in Figure 5,

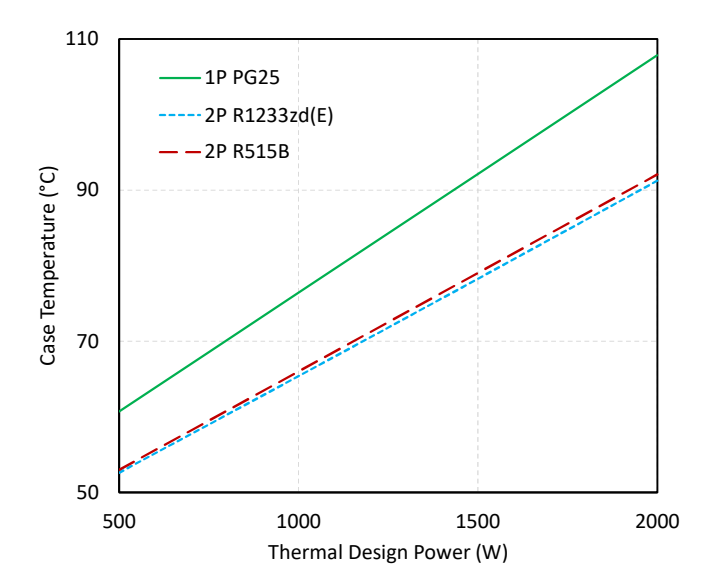


Figure 5: Case temperature variation with TDP for the same microchannel cold plates cooling under both 1P and 2P modes with different working fluids.

since the maximum case temperature is of more concern in practical applications.

Among the two refrigerants modeled for 2P cooling, R1233zd(E) yields lower case temperature than R515B, which is due to the difference in their thermophysical properties. This is different from the experimental results observed in Refs. [13, 22], which is likely because in the experiments of those references, the lower vapor density of R1233zd(E) results in higher vapor line pressure drop and consequently higher inlet subcooling and larger 1P contribution. Nonetheless, both fluids offer lower temperature rise at the cold plate level compared with 1P cooling, which becomes increasingly significant at higher TDPs.

4.2 Condenser Temperature Rise

As discussed before, low pressure drop between the condenser outlet and the reservoir causes points G, H, and A on Figure 3 to converge. Therefore, the refrigerant will be saturated at T_{res} at the condenser outlet. Figure 6 qualitatively shows the temperature plot of both the primary coolant (FW) and the secondary coolant (refrigerant) in a condenser with a countercurrent flow configuration, which is the typical configuration for condensers (usually brazed plate heat exchangers) used in these systems. The FW temperature rises from $T_{FW,in}$ to $T_{FW,out}$ in the condenser with a designed temperature rise of ΔT_{rise} , which then defines the FW flow rate. The refrigerant temperature drops from T_{ci} to T_{res} , due to the saturation temperature drop of ΔT_{sat} induced by the 2P pressure drop across the condenser. Figure 6 also marks the ATD, LMTD, and MTD of the

Figure 6 also marks the ATD, LMTD, and MTD of the condenser. It is noted that Figure 6 is not to-scale, and ATD could be much larger than LMTD when the condenser is highly effective. The ATD equals the difference between the two heat exchanging fluids at the refrigerant outlet side $(T_{res} - T_{FW,in})$, while the LMTD is the average temperature difference between the two fluids along the flow paths in the condenser. As discussed before, although the LMTD is a more thermodynamically accurate representation of the heat exchanger performance, the ATD is of more practical interest to data center engineers. The relationship between ATD and LMTD can be derived from the equation for LMTD [28]:

$$LMTD = \frac{(T_{res} - T_{FW,in}) - (T_{ci} - T_{FW,out})}{\ln \frac{T_{res} - T_{FW,in}}{T_{ci} - T_{FW,out}}}$$
(5)

Rearranging Eq. (5), and using ΔT_{sat} and ΔT_{rise} to represent the temperature change of the two fluids respectively, the ATD can be represented by

$$ATD = \frac{\Delta T_{rise} - \Delta T_{sat}}{1 - \exp\left(-\frac{\Delta T_{rise} - \Delta T_{sat}}{LMTD}\right)}$$
(6)

As shown in Figure 6 and discussed before, MTD represents the difference between the highest refrigerant temperature T_{ci} and the lowest FW temperature $T_{FW,in}$, and $MTD = ATD + \Delta T_{sat}$, which includes the condenser pressure drop-induced saturation temperature drop.

For a given heat exchanger, LMTD is dependent on the HTC values of FW side and refrigerant side, as

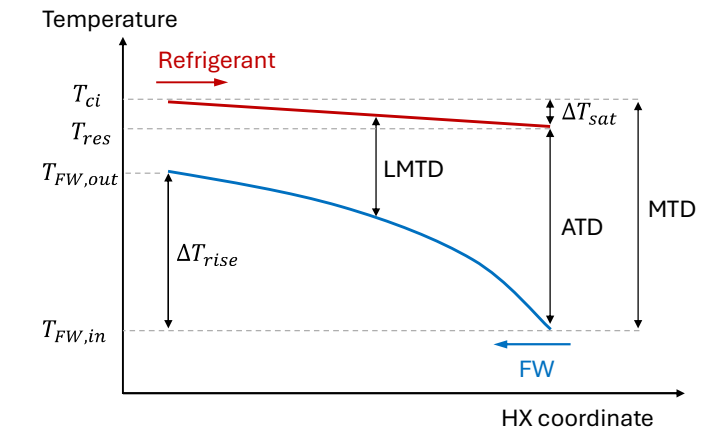


Figure 6: Temperature variation of refrigerant and facility water (FW) in the condenser.

$$LMTD = \frac{Q_{tot}}{UA} \tag{7}$$

where A is the total heat transfer area and U is the overall HTC. U is dependent on the HTC on the primary coolant side, the HTC on the secondary coolant side, and the solid wall conduction. Comparing a 1P DTC HX with a 2P DTC condenser, the primary coolant HTC and the solid conduction can be assumed unchanged. The HTC of refrigerant condensation is within the same order of magnitude as that of 1P water forced convection [28]. In case film-wise condensation of refrigerant yields lower HTC than 1P water convection, the 2P condenser can also be upsized so that the heat transfer area is larger than that for a 1P HX, keeping the UA the same given the same CDU cooling capacity rating. Thus, the LMTD of a condenser in a 2P DTC CDU can be expected to be similar to that of a 1P DTC HX.

In data center cooling operations, the FW flow rate is usually managed to maintain a FW temperature rise ΔT_{rise} of 10 °C, corresponding to 1.5 L/min per kW of heat load for PG25. The refrigerant pressure drop across a condenser is usually within a few psi. Here, we vary the values of condenser pressure drop and condenser LMTD in reasonable ranges, and calculate the ATD and MTD for R1233zd(E) and R515B. Figure 7 shows the variations of ATD and MTD with different condenser pressure drops. The FW temperature rise is fixed at 10 °C, and the LMTD is given as 5 °C. The two fluids have different temperature drop given the same condenser pressure drop. For example, for a given 3 psi condenser pressure drop, R1233zd(E) saturation temperature drops ~2.7 °C, and R515B saturation temperature drops ~0.9 °C. Consequently, ATD and MTD are different for the two fluids.

Figure 7(a) shows that R1233zd(E) results in a lower ATD for a given condenser pressure drop than R515B. For both fluids, the ATD value decreases with increased pressure drop. If ATD is used to evaluate condenser performance for a 2P DTC system, the trend in Figure 7(a) would lead to the conclusions that a higher condenser pressure drop is desirable for a better condenser performance, and a low-pressure fluid R1233zd(E) yields higher performance than a medium-pressure fluid R515B.

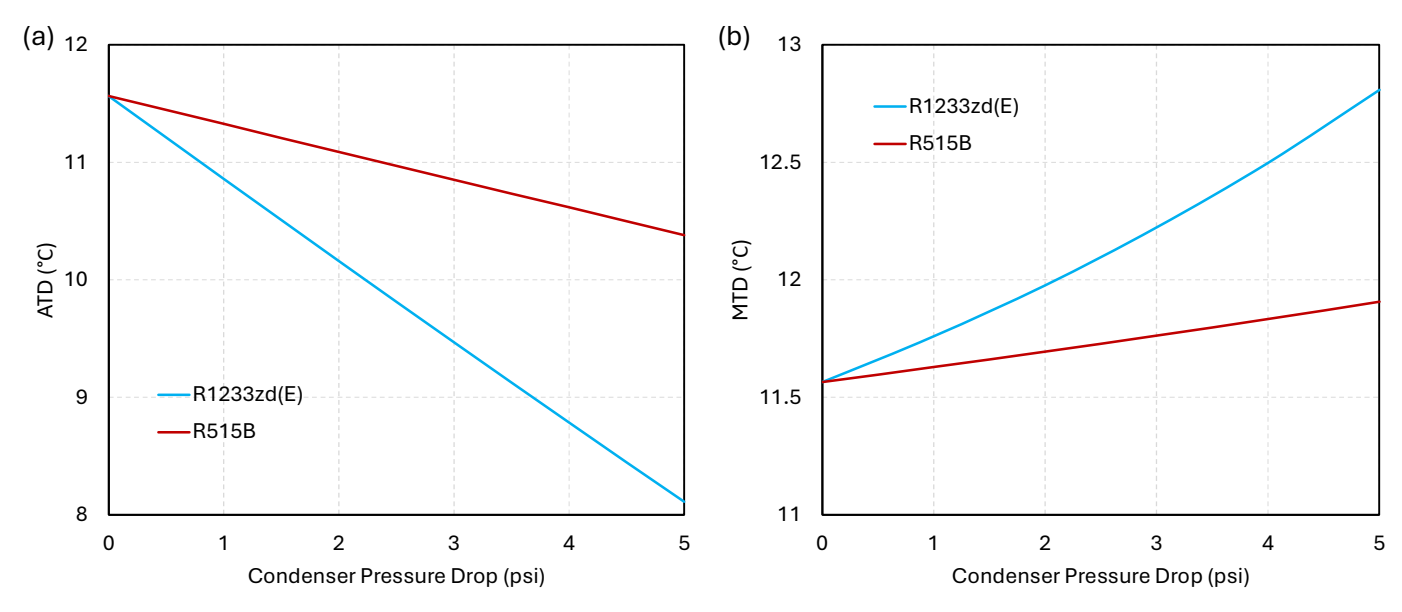


Figure 7: Variations of (a) ATD and (b) MTD with different condenser pressure drop for two refrigerants.

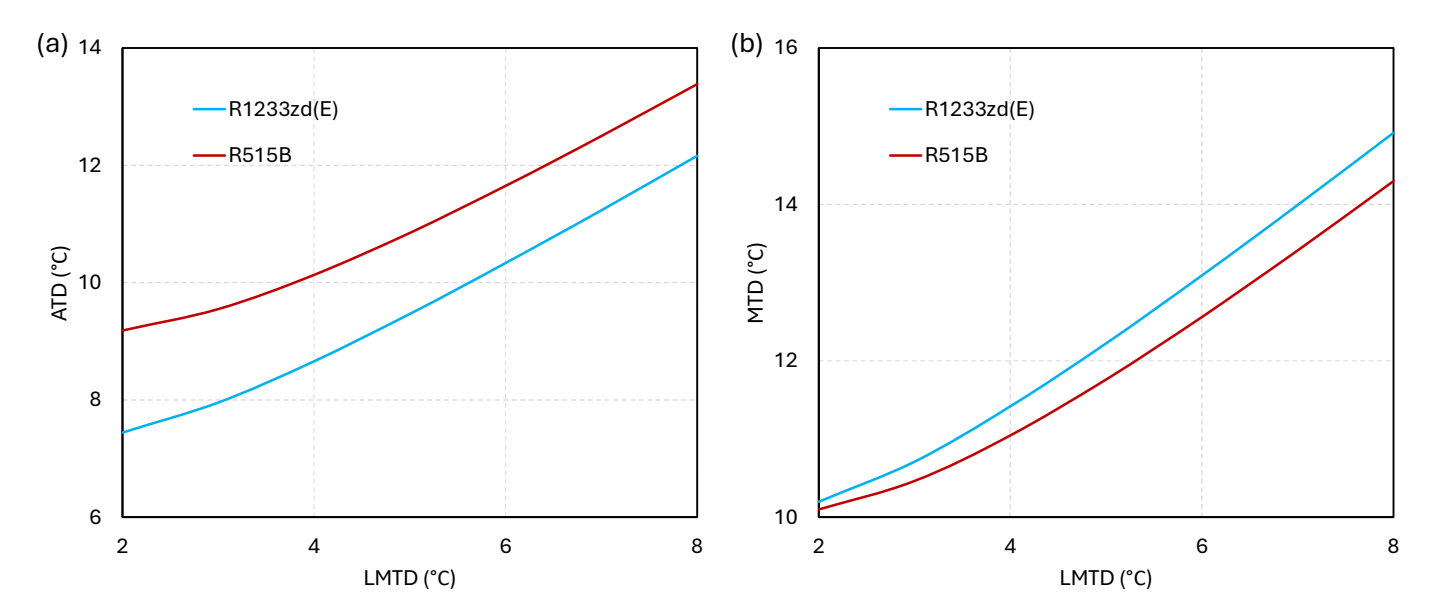


Figure 8: Variations of (a) ATD and (b) MTD with different condenser LMTD for two refrigerants.

The conclusions are counter-intuitive and not thermally reasonable. On the contrary, Figure 7(b) shows that MTD has opposite trends: MTD increases with condenser pressure drop, and R515B yields lower MTD than R1233zd(E). If MTD is used as the performance metric for condensers, opposite conclusions will be drawn. That makes more sense as the MTD value includes contribution from pressure drop within a condenser. Therefore, we suggest that MTD instead of ATD is used for characterizing and comparing condensers for 2P DTC cooling.

Figure 8 shows the variations of ATD and MTD with different LMTD, with a fixed condenser pressure drop of 3 psi and a FW temperature rise of 10 °C. Both ATD and MTD increase with LMTD as expected, since a higher LMTD should

represent worse condenser thermal performance. Again, in Figure 8, R515B results in a higher ATD and a lower MTD than R1233zd(E) given the same LMTD, due to their exclusion and inclusion of pressure drop contributions, respectively. With the LMTD approaching zero, the ATD approaches $(\Delta T_{rise} - \Delta T_{sat})$ and the MTD converges towards ΔT_{rise} , which is consistent with the temperature distribution shown in Figure 6. Because of that, even in an ideal case, when the condenser overall HTC is infinite and there is no pressure drop across the condenser, ATD will be equal to ΔT_{rise} instead of zero. However, for an ideal 1P DTC HX with equal flow rate between primary and secondary fluids, the ATD (= LMTD) becomes zero. Therefore, if one were to compare a 1P DTC HX and a 2P DTC condenser, using the

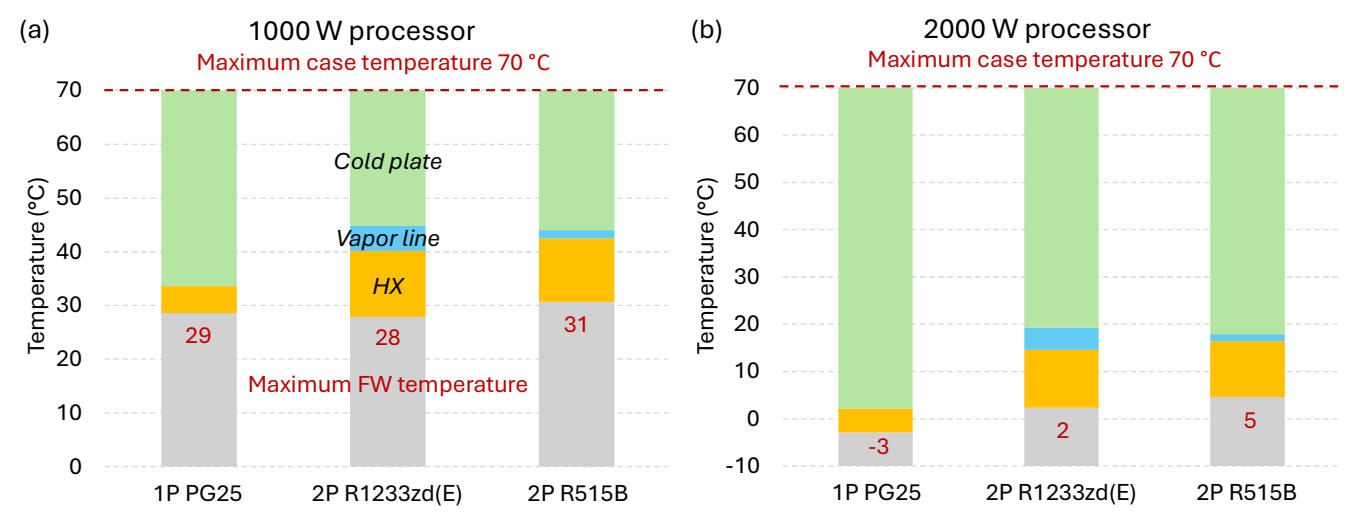


Figure 9: Thermal stack-up plots of DTC cooling for both 1P PG25 and 2P with two refrigerants, given a processor TDP of (a) 1000 W and (b) 2000 W.

ATD value as the metric would lead to the faulty conclusion that even an ideal 2P condenser is inferior although its HTC is already infinite. It is therefore suggested that the MTD should be used as the metric for 2P condenser instead of ATD. Consequently, direct comparison between 2P condenser and 1P HX should be avoided. Instead, they should be compared in a systematic manner, such as using the thermal stack-up of the end-to-end temperature difference as discussed below.

4.3 Thermal Stack-Up

As data center operators are mostly concerned about the end-to-end temperature difference, a thermal stack-up plot would be a good demonstration of the contributing thermal resistances in different cooling technologies [25]. Figure 9 shows the thermal stack-up plots for the two fluids analyzed above in a 2P DTC cooling system, with T_{out} and T_{ci} being the two temperature nodes separating the three thermal resistance contributions. 1P DTC is also plotted for comparison, containing two thermal resistance contributions from cold plate and HX. Figure 9 plots the thermal stack-up for two types of processors: a 1000 W TDP processor and a 2000 W TDP processor, both based on the same footprint case area described in Section 4.1. An arbitrary value of 70 °C is employed as the maximum tolerable case temperature. For 2P refrigerants, the vapor line pressure drop is assumed to be 5 psi, the condenser pressure drop is assumed to be 3 psi, and the condenser LMTD is assumed to be 5 °C. For 1P cooling, the ATD is assumed to be 5 °C. The maximum FW inlet temperature is then obtained by subtracting the end-to-end temperature difference from the maximum case temperature (70 °C). On each stacked bar, the maximum allowable FW temperature is called out on the gray bars. The yellow, blue, and green bars represent the temperature rises due to HX/condenser, vapor line pressure drop, and cold plate, respectively.

Figure 9(a) shows that for a 1000 W processor (corresponding to a heat flux of 121 W/cm²), both 1P DTC and 2P DTC yields similar requirements on FW temperature. R515B allows for a slightly higher FW temperature than R1233zd(E) due to smaller saturation temperature change given the same pressure drop. In real applications, the pressure drop for R515B would be even lower given a similar design [21], which would allow an even higher FW temperature. Comparing 1P and 2P cooling, although there is a smaller temperature rise at the cold plate level for 2P, it is compensated by the higher condenser temperature rise and the additional temperature rise due to vapor line pressure drop. Note that the higher condenser temperature rise is not due to worse thermal performance, since the ATD for 1P cooling and the LMTD for 2P cooling are set to be the same. Instead, it is due to the way the temperature node is defined: the MTD for 2P condenser contains the FW temperature rise contribution. Hence, it is recommended that the comparison of 1P and 2P performance be conducted in a comprehensive manner. focusing on the end-to-end temperature difference. Directly comparing the MTD or ATD for 2P condenser with the ATD for 1P HX could be misleading. Nonetheless, for a 1000 W TDP processor, both 1P and 2P DTC cooling yields similar end-to-end performance, and their practical performance will be dependent on specific design and optimization for respective components in these systems.

Figure 9(b) shows that when the processor power reaches 2000 W (corresponding to a heat flux of 242 W/cm²), the cold plate temperature rise for 1P becomes significantly higher than for 2P, due to the linear relationship between temperature rise and TDP (see Section 4.1). 1P cooling requires a FW temperature below -3 °C, whereas the maximum FW temperature for 2P is 2 °C and 5 °C for R1233zd(E) and R515B, respectively. Additionally, as discussed in Section 4.1, the thermal resistance model of 1P DTC cold plate neglects the temperature non-uniformity across the case surface, and an average case

temperature is captured from the model. When the non-uniformity is taken into account, and considering that the maximum case temperature should be below the 70 °C case temperature threshold, the temperature rise for 1P DTC cold plate would be higher in the thermal stack-up, thus requiring even lower FW temperature. Therefore, it can be expected that with increasing processor TDP above 1000 W, 2P cooling will gradually become inevitable due to its ultrahigh performance at the cold plate level.

It is worth noting that the thermal stack-up in Figure 9 is based on estimation from the models for cold plate and HX described above. Actual 1P and 2P cold plate temperature rise would deviate from the calculated values using heat transfer correlations. The values of ATD for 1P DTC and pressure drop values for 2P DTC are all arbitrary, despite being reasonable. Deviation of these values from those used in this work can be expected. The numbers in Figure 9 are thus not representative of any practical systems. The cold plate temperature rise for both 1P and 2P are modeled for a 25×33 mm² chip package; given the same TDP with a larger die/case surface, i.e., lower heat flux, the cold plate temperature rise will be reduced proportionally to the heat flux, allowing for hotter FW to be implemented in the primary coolant loop. Additionally, the required maximum FW temperature can be further raised by design improvements for both 1P and 2P cooling, such as reducing cold plate base thickness, enhancing cold plate boiling/convection, optimizing the vapor line design (for 2P), and enhancing condenser/HX performance.

5. CONCLUSIONS

In this work, we performed a systematic analysis of the thermal resistances in 2P DTC cooling of data centers. The main conclusions of this paper are listed as follows.

- (1) In 2P DTC cooling systems, the end-to-end temperature difference (ΔT_{e2e}) between processor case temperature T_{case} and FW inlet temperature $T_{FW,in}$ is comprised of three contributions: cold plate thermal resistance, vapor line pressure drop-induced thermal resistance, and condenser thermal resistance.
- (2) The refrigerant temperatures at cold plate outlet T_{out} and at condenser inlet T_{ci} are the two temperature nodes dividing the ΔT_{e2e} . Consequently, the cold plate thermal resistance corresponds to the temperature difference $T_{case} T_{out}$, the vapor line pressure drop-induced thermal resistance corresponds to $T_{out} T_{ci}$, and the condenser thermal resistance corresponds to $T_{ci} T_{FW,in}$ (termed the MTD of a condenser).
- (3) 2P cold plates have lower thermal resistance (and thus lower temperature rise) compared with 1P cold plates, due to the higher HTC of boiling than 1P convection. R1233zd(E) and R515B yields similar thermal resistance given the same working conditions.
- (4) Direct comparison between 2P condenser ATD with 1P HX ATD is not recommended as they have very different fundamental thermal physics. For 2P condensers, ATD is usually much larger than LMTD, due to the temperature

- distribution of the two heat transfer fluids. The MTD introduced here contains the pressure drop induced temperature change and is more representative of the overall condenser performance.
- (5) For a given 2P DTC system, R515B has better performance than R1233zd(E) due to its higher vapor density, because it yields lower vapor line and condenser pressure drops, and also results in lower temperature drop even given the same pressure drop.
- (6) The thermal stack-up plots show that 1P and 2P DTC provides similar thermal performance and requires similar FW temperature when the processor power is 1000 W (heat flux 121 W/cm²). When the processor power reaches 2000 W with the same form factor (heat flux 242 W/cm²), 2P DTC with R515B and R1233zd(E) allows for a ~8 °C and ~5 °C higher FW temperature than 1P DTC, respectively. This difference could be even larger considering that the temperature non-uniformity of 1P cold plate could yield a higher maximum case temperature than the average.

REFERENCES

- [1] A. Shehabi, et al. "2024 United States Data Center Energy Usage Report." (2024).
- [2] "Cooling Operations Optimized for Leaps in Energy, Reliability, and Carbon Hyperefficiency for Information Processing Systems (COOLERCHIPS)." Funding Opportunity Announcement, Advanced Research Projects Agency Energy (ARPA-E), U.S. Department of Energy, 2022.
 - [3] https://www.nvidia.com/en-us/data-center/gb200-nvl72/
- [4] https://www.amd.com/content/dam/amd/en/documents/instinct-tech-docs/product-briefs/instinct-mi325x-datasheet.pdf
- [5] https://www.intel.com/content/www/us/en/content-details/817486/intel-gaudi-3-ai-accelerator-white-paper.html
- [6] D. Kulkarni, et al. "Thermal Performance of Common Cold Plate for Pumped Single- and Two-Phase Direct Liquid Cooling for Next Generation High Power Server Processors." International Electronic Packaging Technical Conference and Exhibition. Vol. 88469. American Society of Mechanical Engineers, 2024.
- [7] https://www.opencompute.org/wiki/Cooling_ Environments/Cold Plate
- [8] K. P. Drummond, et al. "A hierarchical manifold microchannel heat sink array for high-heat-flux two-phase cooling of electronics." International Journal of Heat and Mass Transfer 117 (2018): 319-330.
- [9] C. Woodcock, et al. "Ultra-high heat flux dissipation with Piranha Pin Fins." International Journal of Heat and Mass Transfer 128 (2019): 504-515.
- [10] Q. Wang, et al. "Two-Phase Micropillar Evaporators to Enable Cooling of Next-Generation GPU Servers." 2025 OCP Global Summit Future Technologies Symposium, 2025.
- [11] N. Karwa, and S. Y. Motta. "Low-pressure heat transfer fluids for pumped two-phase cooling." 2021 20th IEEE Intersociety Conference on Thermal and Thermomechanical Phenomena in Electronic Systems (iTherm). IEEE, 2021.

- [12] A. Heydari, et al. "System-Level Assessment of Green Refrigerant Replacements for Direct-to-Chip Two-Phase Cooling." 2024 23rd IEEE Intersociety Conference on Thermal and Thermomechanical Phenomena in Electronic Systems (iTherm). IEEE, 2024.
- [13] Q. Wang, et al. "Performance Comparison of R1233zd(E) and R515B for Two-Phase Direct-to-Chip Cooling", 2025 24th IEEE Intersociety Conference on Thermal and Thermomechanical Phenomena in Electronic Systems (ITherm). IEEE, 2025.
- [14] Q. Wang, et al. "A Server-Level Test System for Direct-To-Chip Two-Phase Cooling of Data Centers Using a Low Global Warming Potential Fluid", 2024 23rd IEEE Intersociety Conference on Thermal and Thermomechanical Phenomena in Electronic Systems (ITherm). IEEE, 2024.
- [15] S. Ozguc, et al. "Design Optimization of Manifold Integrated Skived Cold Plates for Two-Phase Flow-Boiling." 2025 41st Semiconductor Thermal Measurement, Modeling & Management Symposium (SEMI-THERM). IEEE, 2025.
- [16] A. Narayanan, et al. "Investigation of Server Level Direct-to-Chip Two-Phase Cooling Solution for High Power GPUs", International Electronic Packaging Technical Conference and Exhibition. Vol. 88469. American Society of Mechanical Engineers, 2024.
- [17] Q. Wang, and R. W. Bonner. "High-Performance Two-Phase Cooling under Different Cold Plate Orientations", 2025 OCP EMEA Summit Future Technologies Symposium, 2025.
- [18] S. Ozguc, et al. "Investigation of Flow Restrictors for Rack Level Two-Phase Cooling Under Nonuniform Heating." 2024 40th Semiconductor Thermal Measurement, Modeling & Management Symposium (SEMI-THERM). IEEE, 2024.
- [19] S. Ozguc, et al. "Mitigating Flow Maldistribution in Data Center Two-Phase Cooling Systems with Flow Restrictors." Electronics Cooling, 2024.
- [20] A. Heydari, et al. "Controlling Flow Instabilities in Direct-to-Chip Two-Phase Cooling for High Heat Flux Processors." 2023 39th Semiconductor Thermal Measurement, Modeling & Management Symposium (SEMI-THERM). IEEE, 2023.
- [21] R. Tipton, et al. "Maturation of Pumped Two-Phase Liquid Cooling to Commercial Scale-Up Deployment." International Electronic Packaging Technical Conference and Exhibition. Vol. 88469. American Society of Mechanical Engineers, 2024.
- [22] Q. Wang, et al. "Universal Direct-to-Chip Cold Plates for Single- and Two-Phase Cooling", 2024 OCP Global Summit Future Technologies Symposium, 2024.
- [23] D. Kulkarni, et al. "Pumped 2P Refrigerant-Based Direct Liquid Cooling (DLC) Technology for Next Generation AI Clusters with High TDP Accelerators", OCP White Paper, 2025.
- [24] https://accelsius.com/wp-content/uploads/IR80-Spec-Sheet-FINAL.pdf
- [25] R. Curtis, et al. "Performance Comparison of Five Data Center Server Thermal Management Technologies." 2023 39th

- Semiconductor Thermal Measurement, Modeling & Management Symposium (SEMI-THERM). IEEE, 2023.
- [26] Q. Wang, et al. "A Practical Metric for Cold Plate Thermal Performance in Two-Phase Direct-to-Chip Cooling." 2025 41st Semiconductor Thermal Measurement, Modeling & Management Symposium (SEMI-THERM). IEEE, 2025.
- [27] S. G. Kandlikar. "Heat transfer mechanisms during flow boiling in microchannels." Journal of Heat Transfer 126.1 (2004): 8-16.
- [28] T. L. Bergman, Fundamentals of Heat and Mass Transfer. John Wiley & Sons, 2011.
- [29] V. P. Carey. Liquid-vapor phase-change phenomena: an introduction to the thermophysics of vaporization and condensation processes in heat transfer equipment. CRC Press, 2020.